



BIROn - Birkbeck Institutional Research Online

Patel, R.C. and Carter, Andrew (2009) Exhumation history of the Higher Himalayan Crystalline along Dhauliganga-Goriganga river valleys, NW India: new constraints from fission track analysis. *Tectonics* 28 , ISSN 0278-7407.

Downloaded from: <https://eprints.bbk.ac.uk/id/eprint/1744/>

Usage Guidelines:

Please refer to usage guidelines at <https://eprints.bbk.ac.uk/policies.html>
contact lib-eprints@bbk.ac.uk.

or alternatively



BIROn - Birkbeck Institutional Research Online

Enabling open access to Birkbeck's published research output

Exhumation history of the Higher Himalayan Crystalline along Dhauliganga-Goriganga river valleys, NW India: new constraints from fission track analysis

Journal Article

<http://eprints.bbk.ac.uk/1744>

Version: Publisher draft

Citation:

Patel, R.C.; Carter, A. (2009) Exhumation history of the Higher Himalayan Crystalline along Dhauliganga-Goriganga river valleys, NW India: new constraints from fission track analysis – *Tectonics* 28, TC3004

© 2009 AGU

[Publisher version](#)

All articles available through Birkbeck ePrints are protected by intellectual property law, including copyright law. Any use made of the contents should comply with the relevant law.

[Deposit Guide](#)

Contact: lib-eprints@bbk.ac.uk



Exhumation history of the Higher Himalayan Crystalline along Dhauliganga-Goriganga river valleys, NW India: New constraints from fission track analysis

R. C. Patel¹ and A. Carter²

Received 31 July 2008; revised 12 March 2009; accepted 18 March 2009; published 4 June 2009.

[1] New apatite and zircon fission track data collected from two transects along the Dhauliganga and Goriganga rivers in the NW Himalaya document exhumation of the Higher Himalayan Crystalline units. Despite sharing the same structural configuration and rock types and being separated by only 60 km, the two study areas show very different patterns of exhumation. Fission track (FT) data from the Dhauliganga section show systematic changes in age (individual apatite FT ages range from 0.9 ± 0.3 to 3.6 ± 0.5 Ma, $r^2 = 0.82$) that record faster exhumation across a zone that extends from the Main Central Thrust to north of the Vaikrita thrust. By contrast, FT results from the Goriganga Valley show a stepwise change in ages across the Vaikrita thrust that suggests Quaternary thrust sense displacement. Footwall samples yield a weighted mean apatite age of 1.6 ± 0.1 Ma compared to 0.7 ± 0.04 Ma in the hanging wall. A constant zircon fission track age of 1.8 ± 0.4 Ma across both the footwall and hanging wall shows the 0.9 Ma difference in apatite ages is due to movement on the Vaikrita thrust that initiated soon after ~ 1.8 Ma. The Goriganga section provides clear evidence for >1 Ma of tectonic deformation in the brittle crust that contrasts with previous exhumation studies in other areas of the high Himalaya ranges; these studies have been unable to decouple the role of climate erosion from tectonics. One possibility why there is a clear tectonic signal in the Goriganga Valley is that climate erosion has not yet fully adjusted to the tectonic perturbation. **Citation:** Patel, R. C., and A. Carter (2009), Exhumation history of the Higher Himalayan Crystalline along Dhauliganga-Goriganga river valleys, NW India: New constraints from fission track analysis, *Tectonics*, 28, TC3004, doi:10.1029/2008TC002373.

1. Introduction

[2] Formation of the Himalayas following collision between India and Eurasia, at ~ 50 – 55 Ma [*Patriat and*

Achache, 1984; *Garzanti et al.*, 1987; *Rowley*, 1996; *Leech et al.*, 2005], involved shortening within the Indian continental crust [*Molnar and Tapponier*, 1975; *Hodges*, 2000] accommodated mainly along SW directed thrust faults. These faults divide the Himalaya into three main subparallel tectonostratigraphic units, namely, Lesser Himalayas (LHS), Higher Himalayan Crystalline (HHC), and Tethyan Himalayan Series (THS). Each of these units appears to have experienced different exhumation histories that reflect the underlying style of deformation and crust thickening. Interpretations of how crust thickening and deformation have been accommodated differ in that models emphasize the role of gravitationally driven flow and/or pressure-driven flow of hot, weak orogenic crust coupled to surface erosion [*Beaumont et al.*, 2001] or stress the role of deep-rooted slip along thrusts within the orogenic wedge [*Bollinger et al.*, 2006; *Hodges*, 2000]. Defining how convergence between India and Tibet has been and is being accommodated, therefore, rests with understanding how slip is partitioned on the main structures. Studies of brittle fault kinematics and low-temperature exhumation history have suggested that deformation has continued to the present, and the emerging image is that the pattern of active faulting is spatially and temporally variable in addition to out of sequence thrusting [e.g., *Bollinger et al.*, 2006; *Hodges et al.*, 2004]. In this study, low-temperature chronology is used to document the exhumation history of the Himalayan crystalline units in the Garwhal region of the NW Himalaya (Figure 1) to see if, within a single tectonic unit, there are differences along-strike in local brittle deformation that persist over the long term (million year timescale).

[3] The HHC is a 15 to 20 km thick sequence of amphibolite-grade to migmatitic paragneiss sandwiched between the Main Central Thrust (MCT) in the south and the South Tibetan Detachment System (STDS) in the north. Previous low-temperature chronology studies across the Himalayas in western Nepal and NW India [*Blythe et al.*, 2007; *Bojar et al.*, 2005; *Jain et al.*, 2000; *Kumar et al.*, 2003; *Lal et al.*, 1999; *Sorkhabi et al.*, 1996; *Thiede et al.*, 2004, 2005, 2009; *Vannay et al.*, 2004] have shown that the HHC experienced faster exhumation than the adjacent Lesser Himalaya and Tethyan units (Figure 1). Apatite fission track (AFT) ages, which serve as a proxy for exhumation rate, range from 39.9 ± 0.3 [*Schlup et al.*, 2003] to 0.5 ± 0.2 Ma [*Blythe et al.*, 2007] in the THS and 10.1 ± 0.9 [*Thiede et al.*, 2009] to 3.0 ± 0.8 Ma [*Vannay et al.*, 2004] in the LHS. By contrast, within the HHC (MCT hanging wall), AFT ages are consistently younger and range from 4.8 ± 0.4 [*Schlup et al.*, 2003] to 0.3 ± 0.2 Ma [*Blythe*

¹Department of Geophysics, Kurukshetra University, Kurukshetra, India.

²School of Earth Sciences, Birkbeck College, University of London, London, UK.

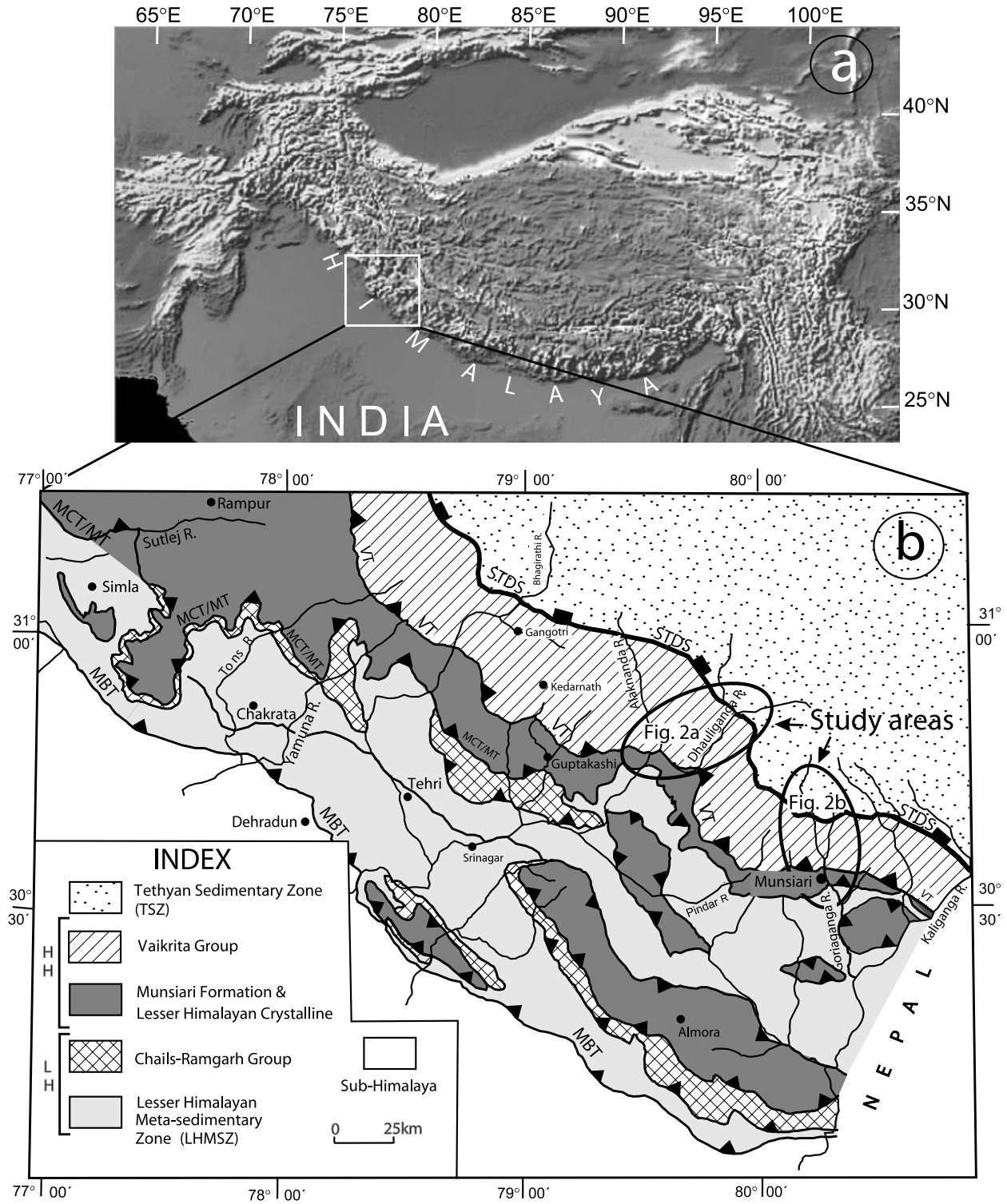


Figure 1. (a) Geological setting of the studied area in the Himalaya (topography based on the GTOPO30 digital elevation model, U.S. Geological Survey). (b) Geological map of the Garhwal and Kumaon Himalayan region of India showing the tectonic setting of the Higher Himalayan Crystalline (HHC) in the overall lithostratigraphic framework of the region (data modified after Paul [1998] and Gururajan and Choudhuri [1999]). The study areas in the Dhauliganga and Goriganga valleys are shown in the oval boxes. STDS, South Tibetan Detachment System; VT, Vaikrita thrust; MCT, Main Central Thrust; MT, Munsiri Thrust; MBT, Main Boundary thrust; HHC, Higher Himalayan Crystalline; and LH, Lesser Himalaya.

et al., 2007]. Differences in AFT exhumation ages within the HHC along strike of the mountain range between Nepal and NW India have been discussed as being due to either a close coupling with precipitation erosion [e.g., *Thiede et al.*, 2004, 2005] or out of sequence tectonics [*Burbank et al.*, 2003], possibly aided by focused monsoon precipitation [*Hodges et al.*, 2004].

[4] The study area is located in the Garhwal (Dhauliganga River valley) and Kumaon (Goriganga River valley) regions of the NW Himalaya (Figure 1b), where two river valleys about 60 km apart run perpendicular to the local strike of the tectonostratigraphic units and bounding structures; that is, the two areas have the same structural configuration. However, the two areas differ in that topographic profiles show the western Dhauliganga Valley has more subdued lower-relief topography compared to the Goriganga Valley (Figure 2). It is unlikely that this difference is due to lithologically controlled variations in erosion as both areas have almost identical rock types, distributed in a similar pattern. Neither is it likely due to any climatic variation, as in the modern sense, the distribution of precipitation is closely similar in both areas [*Bookhagen and Burbank*, 2006], and over the long term this is unlikely to have changed as there is only ~60 km separating the two study areas. Our primary objective is, therefore, to test if these contrasts in landscape reflect underlying differences in tectonic behavior.

2. Geological Setting

[5] The HHC comprises stacked and folded thrust sheets of greenschist- to amphibolite-grade metamorphic rocks generally considered to represent the exhumed leading northeastern portion of the Middle Proterozoic basement of the Indian shield and its cover rocks [*Singh et al.*, 1994; *Rao et al.*, 1995; *V. P. Singh et al.*, Geochronology of the granitic and gneissic rocks from Munsiri, Namik and Tawaghat areas of the Central Crystalline Zone, Kumaon Himalaya, U. P., paper presented at the 3rd National Symposium on Mass Spectrometry, Indian Society for Mass Spectrometry, Hyderabad, India, 1985]. With continental collision between the Indian and the Eurasian plates, southwest directed thrusting along the Vaikrita thrust (VT) [*Valdiya*, 1980; *Davidson et al.*, 1997] and Main Central and Munsiri thrusts (MCT/MT) [*Heim and Gansser*, 1939; *Bouchez and Pecher*, 1981; *Thakur*, 1980; *Jain and Anand*, 1988; *Jain and Manickvasagam*, 1993; *Jain et al.*, 2000; *Searle et al.*, 2008] emplaced HHC rocks over the Lesser Himalayan metasedimentary zone, while normal faulting along the STDS [*Burg and Chen*, 1984; *Herren*, 1987; *Burchfiel et al.*, 1992; *Patel et al.*, 1993] detached the overlying Tethyan Sedimentary Zone (TSZ) from the metamorphic core (Figures 2a and 2b).

[6] The MCT as defined in this study is not equivalent to the MCT of *Bojar et al.* [2005], but it coincides with the Munsiri Thrust [*Heim and Gansser*, 1939; *Gansser*, 1964]. *Bojar et al.* [2005] considered the Vaikrita thrust to be equivalent to the MCT with the MT as another thrust located in a footwall position as part of an imbrication zone, which

incorporates rocks from the HHC (Munsiri Formation) and sediments from the Lesser Himalaya. Recently, it has been suggested that strain criteria are the best tools to define and map the MCT rather than the stratigraphic, lithologic, isotopic, or geochronological criteria [*Searle et al.*, 2008]. Strain analysis and ductile deformation studies from the HHC sequence in Nepal Himalaya [*Searle et al.*, 2008] and NW Himalaya [*Jain and Anand*, 1988; *Jain and Patel*, 1999] show that a wide region of high strain characterizes most of the HHC sequence with a concentration along the bounding margins, i.e., along the top of the STDS and along the base of the MCT. In the study area there is a maximum concentration of different shear strain structures such as S-C fabric, asymmetric augen, and mylonitization located close to the MT, along with an increase in metamorphic grade (inverted metamorphism from biotite to staurolite grade) from the MCT/MT to the VT. On the basis of these observations, the most logical place to map the MCT is along the Munsiri Thrust (MT), which is the base of the broad ductile shear zone and inverted metamorphic sequence within the HHC.

[7] The exposed gneiss and migmatite of the HHC includes the metamorphosed equivalents of the late Proterozoic platform sedimentary sequence and the underlying Proterozoic shield. Previous workers [*Valdiya*, 1980; *Srivastava and Mitra*, 1994; *Ahmad et al.*, 2000] assigned the rocks in the study area to two distinct lithotectonic units: an upper unit, named the Vaikrita Group, and a lower unit, named the Munsiri Formation. The rocks exposed within the Vaikrita group along the Dhauliganga Valley (from south to north) are (1) calc-silicate, quartzite, pelitic gneiss, psammitic gneiss, and biotite schist, (2) psammitic gneiss, (3) migmatite, and (4) sillimanite gneiss (Figure 2a), and along the Goriganga Valley are (1) psammitic, kyanite gneiss, (2) calc-silicate gneiss, (3) garnet-kyanite schist, (4) augen gneiss, and (5) migmatite gneiss (Figure 2b). These metamorphic assemblages were intruded extensively by Miocene age leucogranites [*Valdiya*, 1980; *Roy and Valdiya*, 1988] mainly of bodies of a few meters thick, i.e., not of mapable size. The lower Munsiri Formation comprises low- to medium-grade metamorphic rocks, mainly garnet-bearing mica schists, deformed amphibolites, calc-silicate lenses, quartzites, mylonitic biotite-rich fine-grained gneisses, and augen gneisses. The grade of metamorphism increases (from biotite to staurolite grade) to the north from the MCT/MT to the VT. Kyanite is found in the Vaikrita Group succeeded by sillimanite-grade rocks moving to the north. The sillimanite-bearing gneisses occur in a migmatite zone which is intruded by leucocratic granite bodies of varying dimensions. Farther north kyanite occurs, which is then succeeded by garnet (+ staurolite), biotite, muscovite (+ chlorite), and finally sedimentary rocks of the TSZ. Studies of the HHC show that metamorphic grade decreases from the sillimanite zone up section (northward) as well as down section (southward). So far, there are no U-Th-Pb ages from the study area to date timing of metamorphism, although in the HHC of the Garhwal Himalaya prograde metamorphism is constrained as having occurred between ~44 and 25 Ma [*Foster et al.*, 2000].

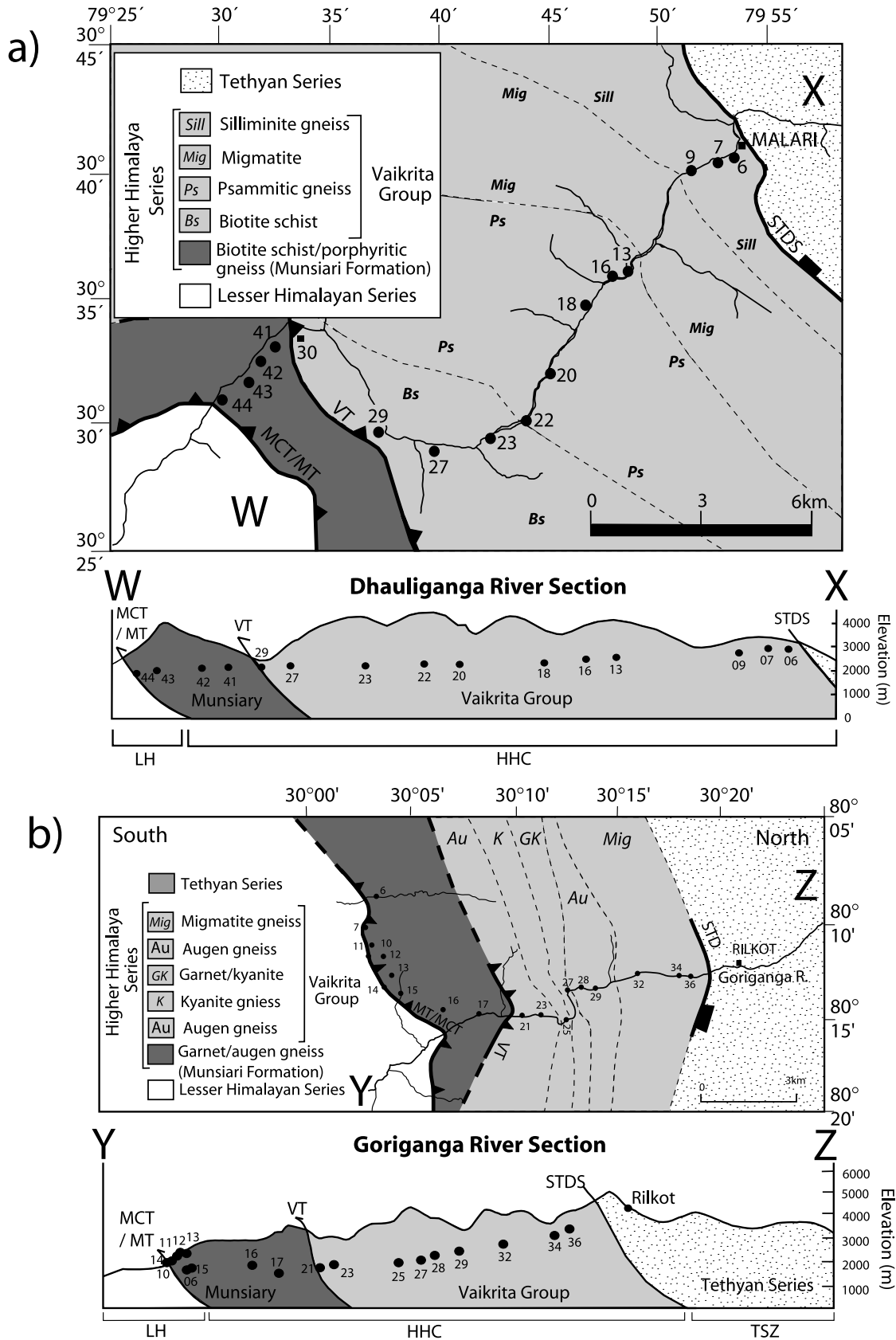


Figure 2. Geological map of the (a) Dhauliganga and (b) Goriganga valleys along with geological cross sections showing sample location based on the sources used in Figure 1.

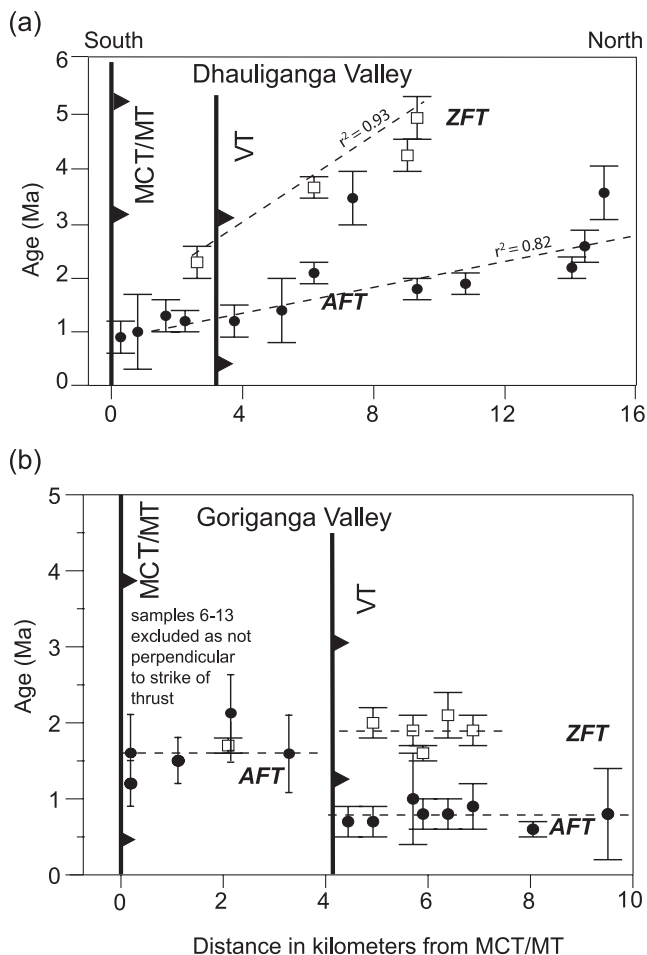


Figure 3. FT age plotted against distance from the MCT/MT to examine for thrust sense displacements. Samples transect shown for (a) the Dhauliganga Valley and (b) the Goriganga Valley. Solid circles represent apatite FT ages, and empty squares represent zircon FT ages. Samples collected along strike are not included.

Elsewhere along the range, the main phase of peak metamorphism and leucogranite emplacement within the HHC occurred during the early Miocene at ~ 23 – 18 Ma [Seitz *et al.*, 1976; Stern *et al.*, 1989; Hubbard and Harrison, 1989; Metcalfe, 1993; Dezes *et al.*, 1999; Searle *et al.*, 1999; Vannay *et al.*, 2004].

3. Thermochronometry

3.1. Fission Track Sample Collection and Analysis

[8] In order to constrain the regional exhumation history, 34 samples were collected along two transects (15 samples from Dhauliganga (Figure 2a) and 19 samples from the Goriganga Valley (Figure 2b)) for fission track analysis. Most samples were collected at or close to the river valley bottom in an attempt to provide a reference point, herein

taken as a constant distance to FT closure isotherm. The aim is to help interpretation by reducing complexity through spatial variations in depth to closure associated with local topography [e.g., Stüwe *et al.*, 1994]. Maximum sample elevation differences ranged between 1.5 and 3 km. The Goriganga Valley samples were collected to extend a previous fission track study made by Bojar *et al.* [2005]. Approximately 20 km long, the north-south sample transects extend from between the MCT/MT in the south and the STDS in the north, crossing one major tectonic boundary, VT, as shown in Figure 3.

[9] Apatite and zircon concentrates were mounted, polished, and etched following standard procedures of the London Fission Track Research Group (apatite etch using 5 N HNO₃ at 20°C for 20 s and zircon etch using KOH-NaOH at 225°C with multiple Teflon mounts for variable durations up to 48 h). Mounts were irradiated with muscovite external detectors and dosimeter glass CN-5 for apatite and irradiated with CN-2 for zircon at the thermal neutron facility of the High Flux Australian Reactor at Lucas Heights in Australia. Fission track densities were measured using an optical microscope at 1250X magnification. Ages ($\pm 1\sigma$) were calibrated by the zeta method [Hurford and Green, 1983], using a zeta factor (analyst R. C. Patel) of 342 ± 11 for apatite and a zeta factor (analyst A. Carter) of 127 ± 5 for zircon, determined by multiple analysis of apatite and zircon standards following the recommendation of Hurford [1990]. Only crystals with prismatic sections parallel to the crystallographic *c* axis were accepted for analysis.

3.2. Results

[10] Fission track results were obtained for 31 apatite samples (13 from the Dhauliganga traverse and 18 from Goriganga) and 14 zircon samples (4 from the Dhauliganga traverse and 10 from the Goriganga traverse (Figure 2 and Table 1)). Since the measured ages were all young (< 5 Ma), with low or zero spontaneous fission track densities, each analysis attempted to sample more than 30–50 grains to obtain a better measure of the spontaneous track density. Although this was not always possible because of a combination of poor apatite yield, highly variable uranium, or abundant fluid inclusions, the data are considered to be of good quality. Track length data were not required since rapid cooling is implicit in such young ages (zero to very low spontaneous track densities also prevent confined track length measurement). Compositional data were not used, as fast cooling removes any resolvable compositional control on fission track annealing. Most FT ages pass the chi-square test (although it should be noted that this test is not reliable for grains with low to zero track counts). Central ages are reported with 1σ error.

3.2.1. Dhauliganga Valley

[11] Apatite FT ages show a well-developed correlation with respect to their distance from the MCT/MT and also with respect to their elevation (Figures 3a and 3b). The youngest age, 0.9 ± 0.3 Ma, is found a few hundred meters north of the MCT/MT, while the oldest age, 3.6 ± 0.5 Ma, is

Table 1. Apatite and Zircon Fission Track Data^a

Sample Reference	Altitude (m)	Latitude	Longitude	Tectonic Unit	Number of Crystals	Dosimeter		Spontaneous		Induced		Age Dispersion		Central Age $\pm 1\sigma$ (Ma)
						ρ_d	N_d	ρ_s	N_s	ρ_i	N_i	$P\chi^2$	RE%	
<i>Dhauliganga Section</i>														
MA-6	2956	N 30° 40.850'	E 79° 53.017'	HHC	43	1.375	9531	0.04015	95	2.856	6351	0.0	67.3	3.6 \pm 0.5
MA-7	2990	N 30° 40.337'	E 79° 51.212'	HHC	34	1.375	9531	0.02787	69	2.482	6360	94.1	0.4	2.6 \pm 0.3
MA-9	2754	N 30° 36.407'	E 79° 48.366'	HHC	27	1.375	9531	0.02874	91	3.104	9850	18.3	14.8	2.2 \pm 0.2
MA-13	2578	N 30° 35.724'	E 79° 47.661'	HHC	45	1.375	9531	0.04163	101	4.853	12,638	3.7	29.3	1.9 \pm 0.2
MA-16	2458	N 30° 40.337'	E 79° 51.212'	HHC	22	1.375	9531	0.05473	125	7.405	16,703	50.4	4.2	1.8 \pm 0.2
MA-16 zircon	2458	N 30° 40.337'	E 79° 51.212'	HHC	20	4.511	3120	1.250	708	6.875	3896	0.0	26.6	5.0 \pm 0.4
MA-18 zircon	2413	N 30° 34.460'	E 79° 46.230'	HHC	20	4.508	3120	0.751	467	4.470	3099	19.6	15.4	4.3 \pm 0.3
MA-20	2160	N 30° 31.564'	E 79° 44.453'	HHC	23	1.375	9531	0.03249	71	2.740	5998	99.6	0.0	3.4 \pm 0.6
MA-22	2165	N 30° 31.564'	E 79° 44.453'	HHC	26	1.375	9531	0.06121	107	6.729	12,315	38.3	3.8	2.1 \pm 0.2
MA-22 zircon	2165	N 30° 31.564'	E 79° 44.453'	HHC	20	4.526	3120	0.914	602	6.932	4675	7.7	13.1	3.7 \pm 0.2
MA-23	2060	N 30° 29.594'	E 79° 41.941'	HHC	11	1.375	9531	0.00984	11	1.673	1809	49.9	2.2	1.2 \pm 0.2
MA-27	1979	N 30° 29.286'	E 79° 39.839'	HHC	42	1.375	9531	0.00590	16	1.117	3148	57.3	6.1	1.2 \pm 0.3
MA-29 zircon	1815	N 30° 29.370'	E 79° 37.360'	HHC	8	4.519	3120	0.475	105	5.535	3120	9.3	18.1	2.3 \pm 0.3
MA-41	1908	N 30° 33.366'	E 79° 32.680'	LHC	21	1.375	9531	0.02900	63	5.547	12,269	73.9	0.7	1.2 \pm 0.2
MA-42	1757	N 30° 32.286'	E 79° 31.510'	LHC	23	1.375	9531	0.00910	16	1.778	2845	79.5	0.6	1.3 \pm 0.3
MA-43	1618	N 30° 31.756'	E 79° 30.907'	LHC	08	1.375	9531	0.00907	02	1.866	0471	94.5	0.0	1.0 \pm 0.7
MA-44	1453	N 30° 31.877'	E 79° 30.933'	LHC	23	1.375	9531	0.00425	08	1.422	2164	69.4	28.1	0.9 \pm 0.3
<i>Goriganga Section</i>														
GR 6	1750	N 30° 02.585'	E 80° 09.076'	LHC	20	1.207	8362	0.089	36	1.753	4840	1.9	14.3	1.5 \pm 0.3
GR 6 zircon	1750	N 30° 02.585'	E 80° 09.076'	LHC	16	4.497	3120	1.599	568	13.11	4717	0.0	23.8	3.4 \pm 0.3
GR-7	2200	N 30° 02.203'	E 80° 10.540'	LHC	15	1.207	8362	0.02504	33	1.887	2664	10.9	20.7	2.9 \pm 0.6
GR-7 zircon	2200	N 30° 02.203'	E 80° 10.540'	LHC	14	4.494	3120	0.781	268	7.596	2558	68.5	0.2	3.0 \pm 0.2
GR-10	2586	N 30° 02.476'	E 80° 11.438'	LHC	47	1.207	8362	0.01588	74	2.731	1207	0.1	76.0	1.3 \pm 0.2
GR-10 zircon	2586	N 30° 02.476'	E 80° 11.438'	LHC	15	4.505	3120	0.462	204	5.022	2274	8.7	16.7	2.6 \pm 0.2
GR-11	2444	N 30° 02.241'	E 80° 10.581'	LHC	26	1.264	8759	0.02289	32	1.793	2684	0.9	35.0	2.7 \pm 0.5
GR-12	2600	N 30° 02.982'	E 80° 11.944'	LHC	28	1.207	8362	0.0182	24	2.381	5235	8.1	20.0	1.0 \pm 0.2
GR-12 zircon	2600	N 30° 02.982'	E 80° 11.944'	LHC	16	4.507	3120	1.002	446	10.52	4408	23.8	0.1	2.9 \pm 0.2
GR-13	2511	N 30° 03.284'	E 80° 12.945'	LHC	12	1.207	8362	0.02359	23	3.407	3326	18.5	4.6	1.4 \pm 0.3
GR-14	2625	N 30° 03.20'	E 80° 13.291'	LHC	31	1.207	8362	0.01135	27	1.776	4549	3.09	18.4	1.2 \pm 0.3
GR-15	2400	N 30° 03.603'	E 80° 13.770'	LHC	16	1.207	8362	0.01101	15	1.905	2938	53.4	2.4	1.1 \pm 0.3
GR-16	1860	N 30° 05.526'	E 80° 14.790'	LHC	27	1.207	8362	0.01014	22	1.192	2676	6.7	59.8	2.1 \pm 0.5
GR-16 zircon	1860	N 30° 05.526'	E 80° 14.790'	LHC	19	4.492	3120	0.295	183	4.972	3157	88.5	0.0	1.7 \pm 0.1
GR-17	1400	N 30° 06.826'	E 80° 15.4'	HHC	16	1.264	8759	0.00855	20	1.538	2960	4.1	80.1	1.2 \pm 0.4
GR-21	1564	N 30° 08.501'	E 80° 15.002'	HHC	13	1.207	8362	0.00850	10	2.807	3052	43.7	9.4	0.7 \pm 0.2
GR-23	1862	N 30° 09.530'	E 80° 15.091'	HHC	21	1.264	8759	0.01153	13	3.782	4311	38.4	4.1	0.7 \pm 0.2
GR-23 zircon	1862	N 30° 09.530'	E 80° 15.091'	HHC	14	4.499	3120	0.3270	153	4.699	2256	6.6	22.0	1.9 \pm 0.2
GR-25	1862	N 30° 10.600'	E 80° 15.140'	HHC	14	1.264	8759	0.00366	05	1.109	0949	41.9	86.6	1.0 \pm 0.6
GR-25 zircon	1862	N 30° 10.600'	E 80° 15.140'	HHC	16	4.486	3120	0.526	226	7.183	3269	0.4	32.0	1.9 \pm 0.2
GR-27	2080	N 30° 11.450'	E 80° 13.758'	HHC	35	1.207	8362	0.00769	26	2.557	8399	6.8	57.0	0.8 \pm 0.6
GR-28	2260	N 30° 11.580'	E 80° 13.587'	HHC	35	1.207	8362	0.00908	42	2.710	1246	6.5	41.6	0.8 \pm 0.2
GR-28 zircon	2260	N 30° 11.580'	E 80° 13.587'	HHC	9	4.485	3120	0.316	107	4.076	1424	9.5	19.7	2.1 \pm 0.3
GR-29	2359	N 30° 12.160'	E 80° 13.420'	HHC	17	1.207	8362	0.01448	19	3.184	4977	0.4	85.0	0.9 \pm 0.3
GR-29 zircon	2359	N 30° 12.160'	E 80° 13.420'	HHC	9	4.488	3120	0.294	179	4.329	2691	0.2	27.8	1.9 \pm 0.2
GR-32	2656	N 30° 14.080'	E 80° 13.000'	HHC	35	1.207	8362	0.01561	66	5.303	2258	2.4	7.6	0.6 \pm 0.1
GR-32 zircon	2656	N 30° 14.025'	E 80° 12.916'	HHC	21	4.492	3120	1.136	732	7.157	4732	0.0	34.3	4.4 \pm 0.4
GR-34	2950	N 30° 16.062'	E 80° 12.997'	HHC	02	1.207	8362	0.00722	02	3.099	0523	46.1	0.0	0.8 \pm 0.6
GR-36		N 30° 16.640'	E 80° 13.320'	HHC	33	1.207	8362	0.01791	30	4.409	8183	5.1	47.9	0.8 \pm 0.2

^aSamples correspond to the letter in the map; ρ is track density ($\times 10^6$ tracks cm^{-2}); N is numbers of tracks counted; subscripts d, s, and i denote tracks in the fluence monitor glass, spontaneous tracks, and induced tracks, respectively. Analyses are by external detector method using 0.5 for the $4\pi/2\pi$ geometry correction factor; ages are calculated using dosimeter glass CN-5; (apatite) $\zeta_{\text{CN5}} = 342 \pm 11$ and CN-2; (zircon) $\zeta_{\text{CN2}} = 127 \pm 5$, calibrated by multiple analyses of IUGS apatite and zircon age standards [see Hurford, 1990]; $P\chi^2$ is probability for obtaining χ^2 value for ν degrees of freedom, where ν is number of crystals minus 1; central age is a modal age, weighted for different precisions of individual crystals [see Galbraith, 1981]. RE% corresponds to the relative error of the central age. Zircon data are shown in bold. HHC is Higher Himalayan Crystalline and LHC is Lesser Himalayan Crystalline units.

found a few hundred meters south of the STDS. Four zircon FT ages also show a similar pattern with the youngest age, 2.3 ± 0.3 Ma, close to the VT and the oldest age, 5.0 ± 0.4 Ma, toward the STDS.

3.2.2. Goriganga Valley

[12] In the Goriganga traverse, apatite FT ages range from 0.7 ± 0.2 to 2.9 ± 0.6 Ma. Two distinct apatite age groups

can be identified, separated by the Vaikrita thrust (Figure 3b). The uniform apatite cooling ages in the hanging wall of VT cluster around 0.8 Ma, while the footwall gives systematically older ages around 1.6 Ma. Zircon FT ages range from 1.6 ± 0.1 to 4.4 ± 0.4 Ma. In the hanging wall of VT the zircon ages have a weighted mean age of 1.8 ± 0.4 Ma, while in the footwall, zircon ages are older ($2.7 \pm$

0.2 Ma). This apparent age difference is linked to inclusion of samples collected along strike of the MCT/MT farther away from the main sample transect. When these data are removed to leave only samples collected along a transect perpendicular to the strike of the thrusts, the remaining single zircon age is seen to be identical (within error) to the zircon ages north of the VT.

4. Exhumation

[13] Low-temperature thermochronology studies in regions to the east and west of the study area show young ages (<5 Ma) diagnostic of rapid cooling, especially for the HHC units [Blythe *et al.*, 2007; Grujic *et al.*, 2006; Jain *et al.*, 2000; Lal *et al.*, 1999; Schlup *et al.*, 2003; Sorkhabi *et al.*, 1996; Thiede *et al.*, 2004, 2005, 2009; Vannay *et al.*, 2004]. Fast cooling suggests high rates of rock uplift and exhumation, but calculation of true rates in such young samples in this type of structural setting (fault/thrust bounded units) is problematic because of the combined influences of topographic wavelength and thermal advection combined with lateral rock transport. High rates of rock uplift cause perturbation of upper crust thermal structure as heat is advected at rates that exceed normal heat loss by conduction, driving isotherms closer to the Earth's surface (e.g., modeling studies of Stüwe *et al.* [1994] and Mancktelow and Grasemann [1997]). Depending on wavelength and amplitude (height), the underlying thermal structure can undulate with the topography, causing the distance between closure isotherm and surface to vary with sample location. Detailed thermal modeling studies show how this can influence the interpretation of low-temperature thermochronometric data, leading to bias in the inferred rates of exhumation [Braun, 2002]. Furthermore, the assumption that rock uplift occurs only in the vertical has been shown to be inappropriate for the high Himalaya, where rock advection also has a strong lateral component; consequently, the distance a sample travels during exhumation may vary according to the location of the closure isotherm and changes in surface slope [see Blythe *et al.*, 2007, Figure 4].

[14] Consideration of the factors outlined above suggests that the combined affects of topography, lateral advection, and the form of the subsurface thermal field can make it difficult to derive true exhumation rates from thermochronometric data. Model simulations performed by Huntington *et al.* [2007] found that where exhumation rates are high, samples collected over a horizontal distance along the direction of lateral transport lead to underestimation of exhumation, but this is generally balanced by the overestimation of exhumation associated with any topographic effects. The net result is an apparent exhumation rate that closely approximates the true vertical component of exhumation. Although lateral transport can cause differences in exhumation paths, when exhumation rates are high, its impact is secondary to thermal advection. This was demonstrated by the 3-D coupled thermokinematic modeling study of Whipp *et al.* [2007], which found no resolvable difference in AFT ages where the sampled slope

faces the thrust vergence, even for a low-angle (<10°) rock trajectory. In the study area the MCT/MT and VT dip due north at ~40–45° along the Dhauliganga and ~30–35° along Goriganga traverses. The STD dips due north ~30–35° along the Dhauliganga and ~35–40° along the Goriganga traverses. Finally, the study of Huntington *et al.* [2007] pointed out that while theoretical considerations suggest lateral components in rock uplift and long-wavelength topography can produce different exhumation paths between samples, the considerable uncertainties attached to young AFT ages (typically 20–50% at 2 σ , as seen in this study) effectively prevent resolution of the different factors. Therefore, the approach adopted in this study is to examine for relative differences in postclosure exhumation and to relate any differences to known structures. Representative erosion rates are derived only for comparison to other published studies.

[15] The above considerations show that a complex 3-D modeling approach is not required to quantify sample exhumation rates for comparison between the two study areas because the FT ages are very young (rapid cooling and extremely high rates of exhumation). Although this condition causes reduced sensitivity to the path of exhumation so that individual sample exhumation rates have little meaning, average exhumation rate data are still useful to compare with other studies across the region. Therefore, we used a 1-D (vertical) approach to thermal modeling to derive average exhumation rates. First, an appropriate closure temperature is defined using the CLOSURE program of Brandon *et al.* [1998] and this value is used in the AGE2EDOT program, as summarized by Ehlers *et al.* [2005], to link measured ages to erosion rates based on the assumption that exhumation occurred at a constant rate under steady state thermal conditions. While AGE2EDOT does not account for transients in the thermal field, resulting in transient shifts in exhumation rate, as long as regional exhumation rates are high, the near-surface thermal field, i.e., FT closure isotherm, will generally quickly adjust to a new steady state (Figure 4). Since exhumation is dominated by erosional advection, the 1-D modeling is based on geothermal gradients values in the range 25–45°C km⁻¹ [e.g., Whipp *et al.*, 2007] and a closure temperature of 135°C that corresponds to the young FT ages (CLOSURE [Brandon *et al.*, 1998]). For thermal conductivity we use the values reported by Ray *et al.* [2007] which range between 2.1 and 3.6 W m⁻¹ K⁻¹, and for heat production we use values reported by Whipp *et al.* [2007] which range between 0.8 and 3.0 μ W m⁻³.

[16] A summary of the results from thermal modeling is presented in Table 2. Models were run using the maximum and minimum values for heat flow, thermal diffusivity, and geothermal gradients since in most cases these inputs are based on assumptions or poorly measured values. Figure 4 plots the results as a function of AFT age and erosion rate. Although the two (maximum and minimum permitted exhumation) growth curves differ (increasingly so with FT age), it can be seen that for the range of AFT ages measured in this study, the attendant age uncertainties span the two curves; that is, there is no resolvable difference as the high rates of exhumation mask the end-member differences in

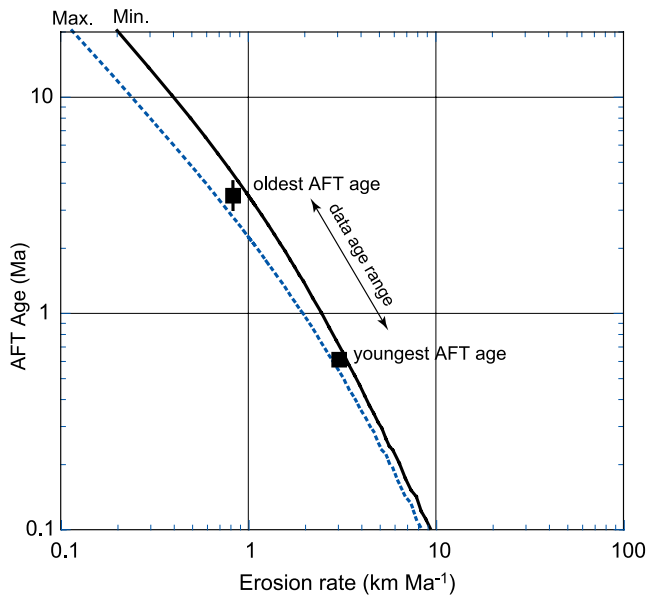


Figure 4. Growth curves of AFT age and erosion rate plotted using AGE2EDOT [Ehlers *et al.*, 2005]. The upper and lower curves represent the maximum and minimum values related to the range of thermal parameters suited to the Himalayas. The AFT ages measured in this study are within error of the two lines.

rock thermal properties considered in this study. For this reason the average of these values is used to derive sample exhumation rate.

5. Interpretation

[17] Using the constraints from thermal modeling, the AFT data from the Dhauliganga Valley yield an average exhumation rate of $1.7 \pm 0.3 \text{ mm a}^{-1}$ which is within error of the data from the Goriganga Valley, where exhumation rates average $2.1 \pm 0.3 \text{ mm a}^{-1}$. This might suggest similar exhumation behavior between the two study areas; however, it more likely reflects reduced sensitivity to the path of exhumation caused by the fast cooling. More informative are the spatial relationships between samples with respect to the main structures (Figure 3). These show clear differences between the distribution of FT ages in the Dhauliganga Valley (apatite FT ages range between 0.9 ± 0.3 and 3.6 ± 0.5 Ma, and zircon FT ages range between 2.3 ± 0.3 and 5.0 ± 0.4 Ma) and the Goriganga Valley (apatite FT ages range between 0.6 ± 0.1 and 2.9 ± 0.6 Ma, and zircon FT ages range between 1.9 ± 0.2 and 4.4 ± 0.4 Ma). Figure 3 plots sample position as a function of distance north of the Main Central Thrust. Only those data that relate to locations perpendicular to the local strike of the main structures are plotted. For the Dhauliganga samples there is a clear trend ($r^2 = 0.82$) of increasing AFT age away from the VT, a trend mirrored by the few zircon fission track (ZFT) ages. By contrast, sample FT ages from the Goriganga Valley show no such trend, maintaining a constant age with distance

north from the VT. South of this thrust, FT ages are slightly older, the opposite to that seen in the Dhauliganga Valley. Such differences cannot be due to lithology since (1) the thermal modeling established that with high rates of exhumation, rock type (thermal conductivity) does not have an important influence on thermal regime as thermal advection is the dominant source of heat transfer and (2) the same rock types are similarly distributed in both areas so that providing rainfall remained the same, there should be no lithological controls on erosion.

[18] Table 2 includes exhumation rates based on the age range values with respect to sample location using the VT as a reference point. The results mirror the age relationships shown by Figure 3. The key differences between the two data sets are that to the north of the VT, Dhauliganga Valley exhumation rates are systematically lower than those seen in the Goriganga Valley and, importantly, the Dhauliganga Valley samples show a systematic increase in exhumation rates southward toward the VT (from 0.8 mm a^{-1} in the north to 2.1 mm a^{-1} in the south). In the Goriganga Valley the spread of exhumation ages is small (from 0.6 to 1.0 Ma) and shows no systematic trend. South of the VT, AFT ages in the Goriganga Valley are older than equivalent samples in the Dhauliganga Valley, where exhumation rates are slightly higher at $\sim 2.6 \pm 0.3 \text{ mm a}^{-1}$. To summarize, in the Dhauliganga Valley, exhumation rates are lower and systematically increase northward away from the VT, while in the Goriganga Valley, exhumation rates are higher and show no systematic trend northward away from the VT. However, exhumation rates are much lower south of the VT in the Goriganga Valley. Two caveats to these exhumation data are that these values must represent minimum estimates of exhumation rates and that transient and spatially variable factors such as fluid advection can also produce signals inconsistent with predictions from simple 1-D steady state thermal models, as seen elsewhere in the Himalayas [Whipp and Ehlers, 2007].

6. Discussion

[19] The AFT ages and rates of exhumation obtained from the Dhauliganga and Goriganga valleys, in general, show a similar range to those documented by recent studies from areas in a similar structural setting, up to 600 km east along strike from western Nepal [Blythe *et al.*, 2007; Jain *et al.*, 2000; Lal *et al.*, 1999; Schlup *et al.*, 2003; Sorkhabi *et al.*, 1996; Thiede *et al.*, 2004, 2005, 2009; Vannay *et al.*, 2004] (Figure 5). However, when the dense array of FT samples are compared, taking into account local structural position, i.e., sample location with respect to the MCT/MT and VT, it is found that there are significant and resolvable differences in exhumation history between the two river sections that point to some form of structural control. Cooling was clearly not simultaneous across each area. The data from the Dhauliganga Valley show a systematic increase in ages (AFT from 0.9 ± 0.3 to 3.6 ± 0.5 Ma, $r^2 = 0.82$ and ZFT from 2.3 ± 0.3 to 5.0 ± 0.4 Ma, $r^2 = 0.98$) with distance northward from the MCT/MT. By contrast, the FT data from the Goriganga Valley show no systematic

Table 2. Exhumation Rates From 1-D Thermal Modelling

River Section and Mineral (Tectonic Unit)	Thermal Diffusivity Range ($\text{km}^2 \text{Ma}^{-1}$)	Internal Heat Production Range ($^\circ\text{C Ma}^{-1}$)	Geothermal Gradient Range ($^\circ\text{C km}$)	FT ^a Cooling Age Range ^b (Ma)	Mean Exhumation Rate ^c (mm a^{-1})	Exhumation Rate Range ($\text{mm a}^{-1} \pm 2\sigma$)	
						South of VT	North of VT
Apatite Zircon	29–50	12–35	25–45	0.9 ± 0.3 to 3.6 ± 0.5	1.7 ± 0.2	2.6 ± 0.3	0.8 ± 0.1 to 2.1 ± 0.3
	29–50	12–35					
Apatite Zircon	29–50	12–35	25–45	0.6 ± 0.1 to 2.9 ± 0.6	2.1 ± 0.3	1.1 ± 0.2 to 2.3 ± 0.3	2.3 ± 0.3 to 3.0 ± 0.4
	29–50	12–35					

^aFT is fission track.^bAll data for FT cooling age range.^cAll data for mean exhumation rate.

trends with respect to distance from structures although there are clear offsets in the age patterns. AFT ages within 4 km of the MCT/MT have a weighted mean age of 1.6 ± 0.1 Ma compared to north of the VT where the weighted mean age is 0.7 ± 0.04 Ma. The few available ZFT data across this area do not mimic this pattern and instead show a single age with a weighted mean value of 1.8 ± 0.4 Ma.

[20] The systematic trend of FT ages in the Dhauliganga Valley, for both zircon and apatite chronometers, suggest that the Dhauliganga region has behaved uniformly since the Pliocene and that no (resolvable) differential movement occurred either side of the VT, although the progressive increase in time difference seen between the AFT and ZFT age trends with distance northward of the VT show exhumation has been faster in the region of the MCT/MT and VT. By contrast, the pattern of ages in the Goriganga Valley shows thrust sense displacement along the VT with resolvable difference in AFT ages either side of the VT. Similar ZFT ages either side of the VT (mean age of 1.8 ± 0.4 Ma) show that displacement must have occurred soon after ~ 2 Ma. The AFT results from the Goriganga Valley in this study are similar to data reported by *Bojar et al.* [2005], who also noted the lack of an age elevation trend in AFT ages. To explain this, they presented geometrical arguments based on the relationships between exhumation path and local slope, noting that when the paleoisotherm is parallel to the surface, there should be no age variation. For the higher-temperature zircon data, *Bojar et al.* [2005] found a positive slope considered diagnostic of tectonic rock uplift rates exceeding erosion, but this was only based on two ZFT ages. In this study five ZFT ages north of the VT are seen to plot on a flat line consistent with the AFT data, although the data points do not extend across the whole sample transect (Figure 3b).

[21] Since FT ages reflect the combination of distance that a rock particle has traveled between closure isotherm and surface and exhumation velocity, any age differences must be due to variable distance and/or velocity. Similar ages imply that velocity and distance were the same across the sampled sites; that is, isotherms are parallel to the surface slope. There are clear differences in exhumation history between the two study areas, and while thrust sense displacement might account for some of these differences, variation in regional erosion may also be important. The western Dhauliganga Valley has more subdued lower-relief topography compared to the Goriganga Valley, so that it is conceivable that spatially variable rainfall might account for some of the differences between the Goriganga and Dhauliganga data sets given that regional topography is similar across the two study sites. Any sustained difference in rainfall should directly translate into significant differences in stream power (given the similar sized drainages). However, we discount climate control on erosion on the basis that the Dhauliganga Valley is located only 60 km to the west of the Goriganga Valley, and it is hard to envisage how a major change in monsoon precipitation can occur over such a short distance, especially where (at the regional scale) the distribution of topography is broadly similar. Modern rainfall intensity and distribution across the

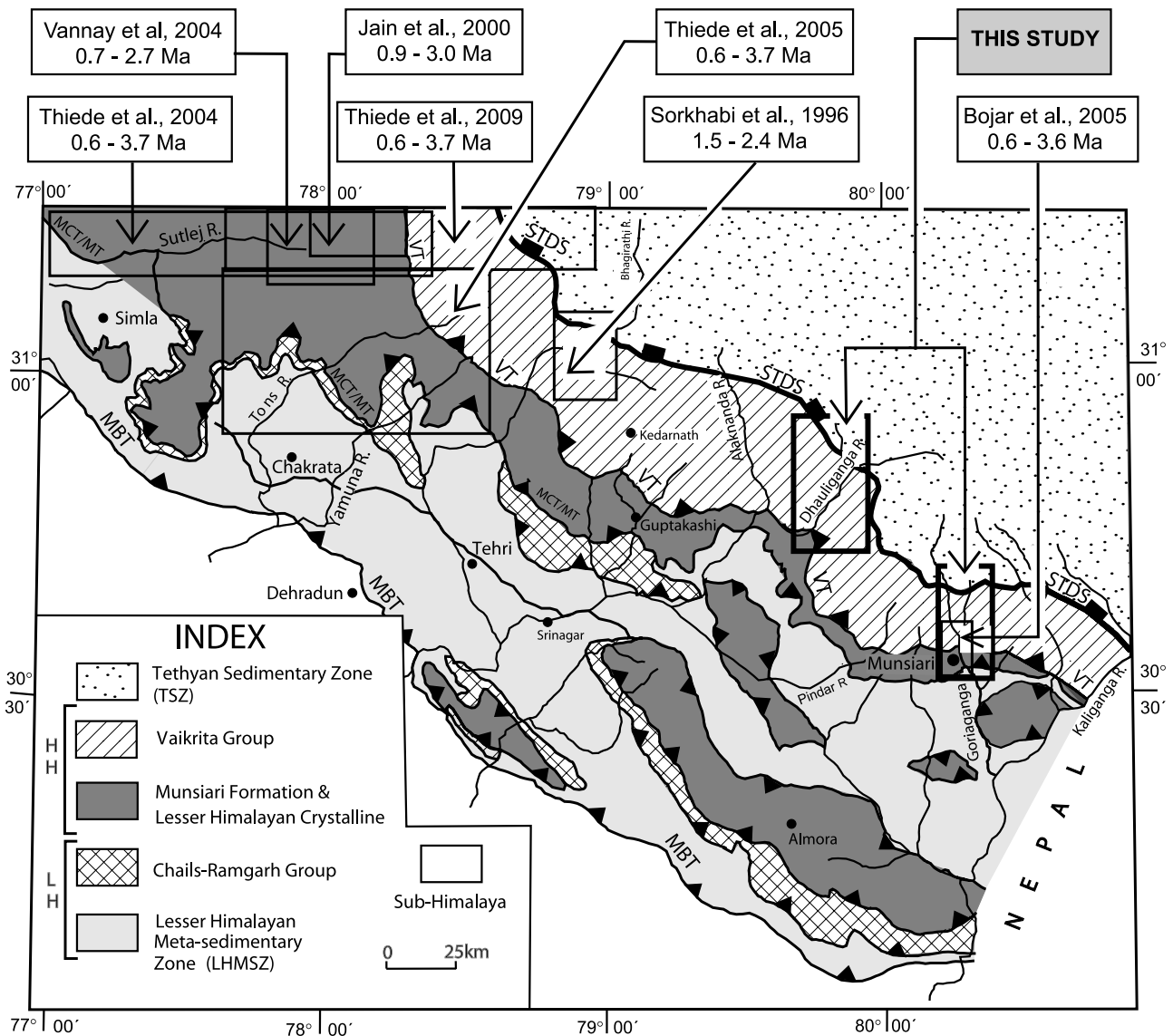


Figure 5. Map showing the AFT ages on samples collected from similar structural locations to the west of the study area. A similar age range of AFT data is observed for ~600 km along strike.

two study areas support this and show no significant difference [Bookhagen and Burbank, 2006] (Figure 6), although it is questionable whether modern observations are useful when comparing to data that relate to million year timescales.

[22] The differences in AFT ages seen across the VT in the Goriganga section rate are consistent with thrust sense displacements. The age offsets allow the rate of slip to be estimated as there are no differences in sample ages within the hanging wall and footwall, indicating that depths to closure isotherms are constant in both units. Using the thermal parameters in the 1-D modeling (section 4 and Table 2) with an average surface temperature of 5°C, closure at 0.7 Ma would give an average thrust slip rate of ~2–3 mm a⁻¹. Consideration of system response times to tectonic and climate perturbations using simplified

analytical steady state models [Whipple and Meade, 2004] shows that rock uplift can rapidly adjust to climatic perturbations, but a longer response time is needed to adjust to transients in local tectonics [Whipple and Meade, 2006]. This finding supports the idea that the apparent differences in topographic relief between the two study areas relate to the longer response time of erosion adjusting to a tectonically driven increase in rock uplift rather than local variations in climate (given there is no evidence in the modern precipitation data to support this).

6.1. Comparison With Adjacent Regions

[23] Consequent with increasing numbers of low-temperature (brittle crust) exhumation studies of the Himalayas has been a growing appreciation that exhumation of the HHC has been rapid and similar along strike [Blythe et

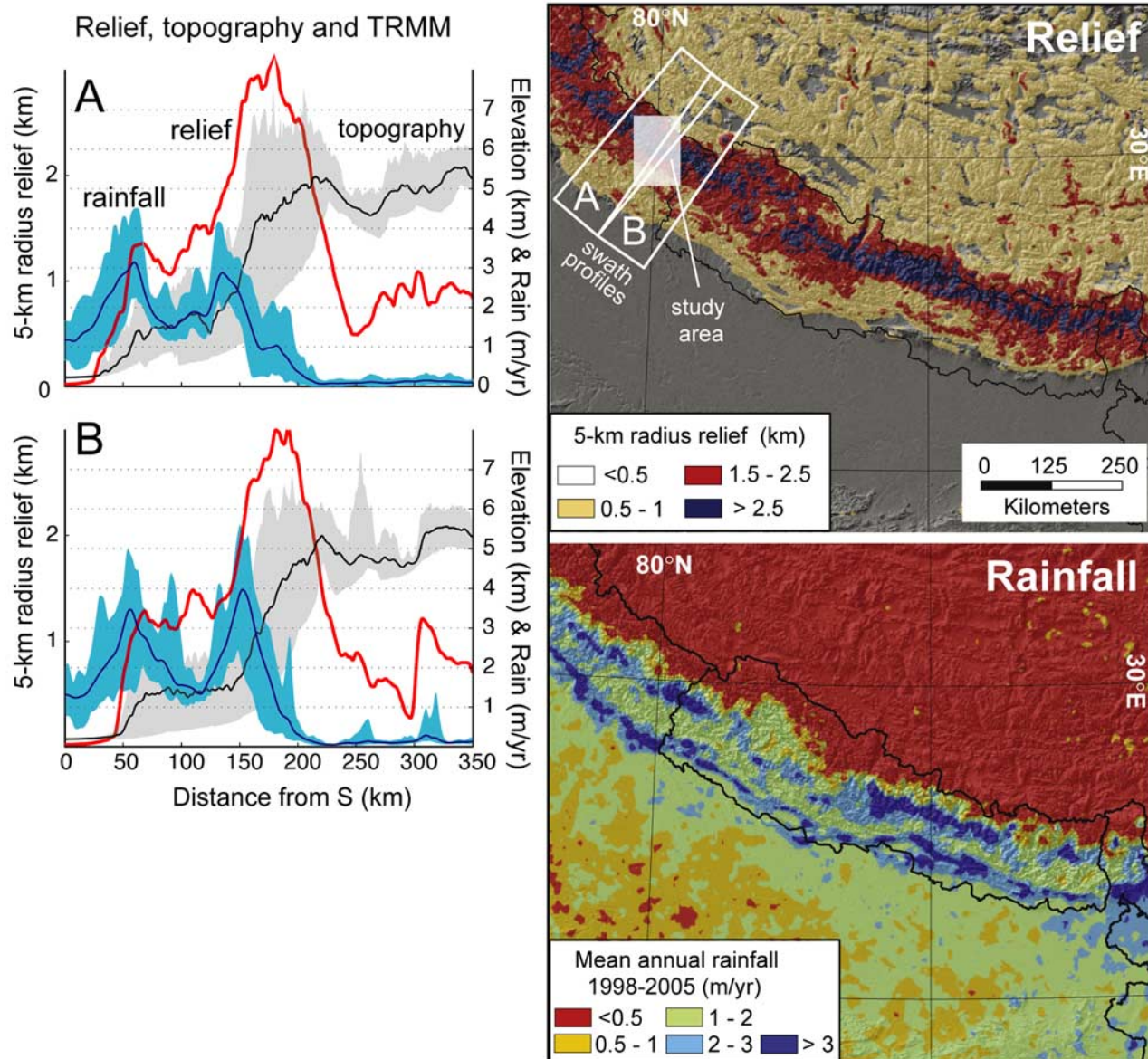


Figure 6. Plots of topography, relief, and Tropical Rainfall Measurement Mission (TRMM)-derived rainfall variations for the study region [from *Bookhagen and Burbank, 2006*]. The TRMM-based monsoon rainfall amounts are averaged from January 1998 to December 2005. The 5 km radius relief is calculated from topographic data merged from Shuttle Radar Topography Mission V2, Digital Terrain Elevation Data, and Atmosphere-Surface Turbulent Exchange Research Facility-digital elevation model imagery with a spatial resolution of 90 m.

al., 2007; *Burbank et al.*, 2003; *Thiede et al.*, 2004, 2005, 2009]. Apart from Bhutan, where 5–10 Ma AFT ages are linked to local orographic disturbance by the Shillong Plateau [*Grujic et al.*, 2006], most studies record AFT ages from the HHC that are <5 Ma. A recent compilation of 241 low-temperature chronometric ages in the northwest Himalaya by *Thiede et al.* [2009], west of this study (Figure 5), highlights the degree of this similarity in AFT ages by recognizing a 40–80 km wide band between the MCT/MT and STD of mostly HHC units that experienced high ($>2 \text{ mm a}^{-1}$) exhumation

rates since ~ 4 Ma. Despite a similar range of ages there are also local spatial variations in exhumation, but the underlying cause is not clear because of the uncertainties attached to relating present-day climate and precipitation to the geologic past combined with variable locations of samples with respect to local thermal structure (topography) and structural boundaries. For example, AFT data from Nepal suggest that slip may have occurred on the MCT during the past 1 Ma, but there is a caveat that climate change may have had a role in the pattern of exhumation [*Blythe et al.*, 2007]. The results

from this study suggest that in some areas, with careful strategic sampling, it is possible to extract less ambiguous evidence for localized tectonic control on exhumation.

[24] While apatite FT data from across the NW Himalaya and between the MCT/MT and STD are closely similar, this is not the case for ZFT data that record closure from higher temperatures and greater crustal depth. ZFT ages produced in this study from the hanging wall of the VT are <6 Ma, which is noticeably different from data in a similar structural setting from the Sutlej region to the NW where the ZFT ages are between 10 and 12 Ma [Yannay *et al.*, 2004]. The age difference between these locations points to an eastward along-strike increase in the depth and rate of exhumation. ZFT data from Nepal to the east of the study area are even younger (<2 Ma), suggesting this may be a systematic trend. An along-strike increase in exhumation has potentially significant implications for how strain deformation and brittle deformation have been partitioned over the long term, but as yet, the data coverage is insufficient to confirm if this apparent trend is real. New ZFT data are required between the MCT/MT and STD in westernmost Nepal and the area between 79°E and 80°E .

6.2. Wider Implications

[25] Exactly how convergence of India has been accommodated across the entire orogen is not well understood, hence, the diverse range of mechanical and thermomechanical models that have been put forward over the last 30 years [Yin, 2006, and references therein]. Most models highlight rapid exhumation of the HHC relative to the surrounding rocks and emphasize the role of ductile flow. Recent thermomechanical models couple ductile flow of the HHC with surface erosion, since along the southern topographic front, monsoon rains are at their most intense, e.g., the channel flow model of Beaumont *et al.* [2001]. This process requires the faults and shear zones that define the boundaries to the HHC, i.e., the STD and MCT, to be active during flow, but it is unclear how these fault zones have facilitated exhumation in the brittle uppermost portions of the crust. Our results show that while climate must have a major influence on exhumation in the brittle crust, there must also be local tectonic control on rock uplift. We emphasize local control because two similarly orientated transects across the high Himalayas only 60 km apart show very different exhumation signals that cannot be explained by change in climate erosion. Previous studies have considered the role of Quaternary out of sequence active thrusting at the topographic front and proposed a positive feedback between focused erosion and deformation of the Higher Himalayan Ranges [Hodges *et al.*, 2004]. The

evidence from this study precludes such a mechanism on the basis that slip on the VT in the Goriganga section appears to have been ongoing for nearly 2 Ma, while in a similar orographic location the Dhauliganga results show no evidence for local thrust sense displacement.

7. Conclusions

[26] Despite considerable effort, previous exhumation studies along the Himalayan front have, as yet, been unable to find unambiguous evidence for tectonic control on exhumation of the high Himalaya, due largely to strong coupling between brittle tectonics and climate erosion. The results presented in this study document the cooling and exhumation history of two structurally identical sections of the HHC exposed along the Dhauliganga and Goriganga river valleys in the NW Himalaya. Although both river sections are separated by only 60 km and share the same climate, they have experienced very different exhumation histories. FT data from the Dhauliganga River valley show systematic changes in age passing from the south to the north (individual apatite FT ages range from 0.9 ± 0.3 to 3.6 ± 0.5 Ma, $r^2 = 0.82$, and zircon FT ages range from 2.3 ± 0.3 to 5.0 ± 0.4 Ma, $r^2 = 0.98$) which reflect faster exhumation, but not differential slip, across a zone that extends from the Main Central Thrust to beyond the Vaikrita thrust. In the Goriganga Valley, uniform apatite ages in the footwall of the Vaikrita thrust give a weighted mean age of 1.6 ± 0.1 Ma, while samples collected at distances across the hanging wall give the same apatite ages, which have a weighted mean age of 0.7 ± 0.04 Ma. A constant ZFT age of 1.8 ± 0.4 Ma across both footwall and hanging wall of the Vaikrita thrust shows that offset in apatite ages (from 1.6 to 0.7 Ma) must have occurred after zircon closure at ~ 1.8 Ma. Such recent slip on the Vaikrita thrust, which is estimated to have occurred at rates in excess of $\sim 2\text{--}3$ mm a^{-1} , might explain why the pattern of topographic relief differs between the two study areas since system response times to tectonic perturbations have been shown to take longer than any adjustments to transient changes in climate [Whipple and Meade, 2006].

[27] **Acknowledgments.** The manuscript was much improved by the careful reviews of Todd Ehlers, Rasmus Thiede, and Kate Huntington. This study was supported by Department of Science and Technology, India Research Project DST/23(373)/SU/2003 and ESS/16/242/2005/Kameng/03, and British Council and Commonwealth Institute Academic Fellowship awards to R. C. Patel. A. K. Jain, S. Singh, N. Lal, and Y. Kumar are sincerely thanked for their ongoing support.

References

- Ahmad, T., N. Harris, M. Bickle, H. Chapman, J. Bunbury, and C. Prince (2000), Isotopic constraints on the structural relationships between the Lesser Himalayan Series and the High Himalayan Crystalline Series, Garhwal Himalaya, *Geol. Soc. Am. Bull.*, *112*, 467–477, doi:10.1130/0016-7606(2000)112<0467:ICOTSR>2.3.CO;2.
- Beaumont, C., R. A. Jamison, M. H. Nguyen, and B. Lee (2001), Himalayan tectonics explained by extrusion of a low-viscosity crustal channel coupled to focused surface denudation, *Nature*, *414*, 738–742, doi:10.1038/414738a.
- Blythe, A. E., D. W. Burbank, A. Carter, K. Schmidt, and J. Putkonen (2007), Plio-quaternary exhumation history of the central Nepalese Himalaya: I. Apatite and zircon fission track and apatite [U-Th]/He analysis, *Tectonics*, *26*, TC3002, doi:10.1029/2006TC001990.
- Bojar, A.-V., H. Fritz, S. Nicolescu, M. Bregar, and R. P. Gupta (2005), Timing and mechanisms of central Himalayan exhumation: Discriminating between tectonic and erosion processes, *Terra Nova*, *17*, 427–433, doi:10.1111/j.1365-3121.2005.00629.x.
- Bollinger, L., P. Henry, and J. P. Avouac (2006), Mountain building in the Nepal Himalaya: Thermal and kinematic model, *Earth Planet. Sci. Lett.*, *244*, 58–71, doi:10.1016/j.epsl.2006.01.045.

- Bookhagen, B., and D. W. Burbank (2006), Topography, relief, and TRMM-derived rainfall variations along the Himalaya, *Geophys. Res. Lett.*, **33**, L08405, doi:10.1029/2006GL026037.
- Bouchez, J.-L., and A. Pecher (1981), The Himalayan Main Central Thrust pile and its quartz rich tectonics in central Nepal, *Tectonophysics*, **78**, 23–50, doi:10.1016/0040-1951(81)90004-4.
- Brandon, M., M. Roden-Tice, and J. Garver (1998), Late Cenozoic exhumation of the Cascadia accretionary wedge in the Olympic Mountains, northwestern Washington State, *Geol. Soc. Am. Bull.*, **110**, 985–1009, doi:10.1130/0016-7606(1998)110<0985:LCEOTC>2.3.CO;2.
- Braun, J. (2002), Estimating exhumation rate and relief evolution by spectral analysis of age-elevation datasets, *Terra Nova*, **14**, 210–214, doi:10.1046/j.1365-3121.2002.00409.x.
- Burbank, D. W., A. E. Blythe, J. K. Putkonen, B. A. Pratt-Sitaula, E. J. Gabet, M. E. Oskin, A. P. Barros, and T. P. Ojha (2003), Decoupling of erosion and precipitation in the Himalaya, *Nature*, **426**, 652–655, doi:10.1038/nature02187.
- Burchfiel, B. C., C. Zhiliang, K. V. Hodges, L. Yuping, L. H. Royden, D. Changrong, and X. Jiene (1992), The south Tibetan detachment system, Himalayan orogen: Extension contemporaneous with and parallel to shortening in a collisional mountain belt, *Spec. Pap. Geol. Soc. Am.*, **269**, 1–44.
- Burg, J. P., and G. M. Chen (1984), Tectonics and structural zonation of southern Tibet, *Nature*, **311**, 219–223, doi:10.1038/311219a0.
- Davidson, C., D. E. Gruijic, L. S. Hollister, and S. M. Schmid (1997), Metamorphic reactions related to decompression and synkinematic intrusion of leucogranite, High Himalayan Crystallines, Bhutan, *J. Metamorph. Geol.*, **15**, 593–612, doi:10.1111/j.1525-1314.1997.0044.x.
- Dezes, P. J., J. C. Vannay, A. Steck, F. Bussy, and M. Cosca (1999), Synorogenic extension: Quantitative constraints on the age and displacement of the Zaskar shear zone (northwest Himalaya), *Geol. Soc. Am. Bull.*, **111**, 364–374, doi:10.1130/0016-7606(1999)111<0364:SEQCOT>2.3.CO;2.
- Ehlers, T. A., et al. (2005), Computational tools for low-temperature thermochronometer interpretation, *Rev. Mineral. Geochem.*, **58**, 589–622, doi:10.2138/rmg.2005.58.22.
- Foster, G., P. Kinny, D. Vance, C. Prince, and N. Harris (2000), The significance of monazite U-Th-Pb age data in metamorphic assemblages: A combined study of monazite and garnet chronometry, *Earth Planet. Sci. Lett.*, **181**, 327–340, doi:10.1016/S0012-821X(00)00212-0.
- Galbraith, R. F. (1981), On statistical models for fission track counts, *Math. Geol.*, **13**, 471–478, doi:10.1007/BF01034498.
- Gansser, A. (1964), *Geology of the Himalayas*, 289 pp., Interscience, London.
- Garzanti, E., A. Baud, and G. Mascle (1987), Sedimentary record of the northward flight of India and its collision with Eurasia (Ladakh Himalaya, India), *Geodin. Acta*, **1**, 297–312.
- Gruijic, D., I. Coutand, B. Bookhagen, S. Bonnet, A. Blythe, and C. Duncan (2006), Climatic forcing of erosion, landscape, and tectonics in the Bhutan Himalayas, *Geology*, **34**, 801–804, doi:10.1130/G22648.1.
- Gururajan, N. S., and B. K. Choudhuri (1999), Ductile thrusting, metamorphism and normal faulting in Dhauliganga Valley, Garhwal Himalaya, *Himalayan Geol.*, **20**, 19–29.
- Heim, A., and A. Gansser (1939), Central Himalaya, *Soc. Helv. Sci. Nat.*, **73**, 1–245.
- Herren, E. (1987), Zaskar shear zone: Northeast-southwest extension within the Higher Himalaya (Ladakh, India), *Geology*, **15**, 409–413, doi:10.1130/0091-7613(1987)15<409:ZSNEW>2.0.CO;2.
- Hodges, K. V. (2000), Tectonics of the Himalaya and southern Tibet from two perspectives, *Geol. Soc. Am. Bull.*, **112**, 324–350, doi:10.1130/0016-7606(2000)112<0324:TOTHAS>2.3.CO;2.
- Hodges, K. V., C. Wobus, K. Ruhl, T. Schildgen, and K. Whipple (2004), Quaternary deformation, river steepening, and heavy precipitation at the front of the Higher Himalayan ranges, *Earth Planet. Sci. Lett.*, **220**, 379–389, doi:10.1016/S0012-821X(04)00063-9.
- Hubbard, M. S., and T. M. Harrison (1989), $^{40}\text{Ar}/^{39}\text{Ar}$ age constraints on deformation and metamorphism in the MCT zone and Tibetan slab, eastern Nepal Himalaya, *Tectonics*, **8**, 865–880, doi:10.1029/TC0081004p00865.
- Huntington, K. W., T. A. Ehlers, K. V. Hodges, and D. M. Whipp Jr. (2007), Topography, exhumation pathway, age uncertainties, and the interpretation of the thermochronometer data, *Tectonics*, **26**, TC4012, doi:10.1029/2007TC002108.
- Hurford, A. J. (1990), Standardization of fission track dating calibration: Recommendation by Fission Track Working Group of IUGS Subcommittee on Geochronology, *Chem. Geol.*, **80**, 171–178.
- Hurford, A. J., and P. F. Green (1983), The zeta age calibration of fission-track dating, *Chem. Geol.*, **41**, 285–317.
- Jain, A. K., and A. Anand (1988), Deformational and strain patterns of an intracontinental collision ductile shear zone—An example from the Higher Garhwal Himalaya, *J. Struct. Geol.*, **10**, 717–734, doi:10.1016/0191-8141(88)90079-X.
- Jain, A. K., and R. M. Manickvasagam (1993), Inverted metamorphism in the intracontinental ductile shear zone during Himalayan collision tectonics, *Geology*, **21**, 407–410, doi:10.1130/0091-7613(1993)021<0407:IMTID>2.3.CO;2.
- Jain, A. K., and R. C. Patel (1999), Structure of the Higher Himalayan Crystallines along the Suru-Doda valleys (Zaskar), NW Himalaya, in *Geodynamics of the NW Himalaya, Gondwana Res. Group Mem.*, vol. 6, edited by A. K. Jain and R. M. Manickvasagam, pp. 91–110, Field Sci., Osaka, Japan.
- Jain, A. K., D. Kumar, S. Singh, A. Kumar, and N. Lal (2000), Timing, quantification, and tectonic modelling of Pliocene-Quaternary movements in the NW Himalaya: Evidences from fission track dating, *Earth Planet. Sci. Lett.*, **179**, 437–451, doi:10.1016/S0012-821X(00)00133-3.
- Kumar, D., A. K. Jain, R. C. Patel, and N. Lal (2003), Exhumation of the Himalayan metamorphic belt (HMB): Role of crustal-scale folds as revealed from fission track ages, *Newsl. Geol. Cont. Stud. India* **13**(1), pp. 18–20, Dep. of Sci. and Technol., Gov. of India, New Delhi.
- Lal, N., Y. P. Mehta, D. Kumar, A. Kumar, and A. K. Jain (1999), Cooling and exhumation history of the Mandi granite and adjoining tectonic units, Himachal Pradesh, and estimation of closure temperature from external surface of zircon, in *Geodynamics of the NW Himalaya, Gondwana Res. Group Mem.*, vol. 6, edited by A. K. Jain and R. M. Manickvasagam, pp. 207–216, Field Sci., Osaka, Japan.
- Leech, M. L., S. Singh, A. K. Jain, S. L. Klempner, and R. M. Manickvasagam (2005), The onset of India-Asia continental collision: Early, steep subduction required by the timing of UHP metamorphism in the western Himalaya, *Earth Planet. Sci. Lett.*, **234**, 83–97, doi:10.1016/j.epsl.2005.02.038.
- Mancktelow, N. S., and B. Grasemann (1997), Time-dependent effects of heat advection and topography on cooling histories during erosion, *Tectonophysics*, **270**, 167–195, doi:10.1016/S0040-1951(96)00279-X.
- Metcalfe, R. P. (1993), Pressure, temperature, and time constraints on metamorphism across the Main Central Thrust zone and high Himalayan slab in the Garhwal Himalaya, in *Himalayan Tectonics*, edited by P. J. Treloar and M. P. Searle, *Geol. Soc. Spec. Publ.*, **74**, 485–509.
- Molnar, P., and P. Tapponnier (1975), Cenozoic tectonics of Asia: Effects of a continental collision, *Science*, **189**(4201), 419–426, doi:10.1126/science.189.4201.419.
- Patel, R. C. (1991), Strain geometry and strain patterns of the collision zone, Zaskar, NW Himalaya, Ph.D. thesis, 219 pp., Dep. of Earth Sci., Univ. of Roorkee, Roorkee, India.
- Patel, R. C., S. Sandeep, A. Asokan, R. M. Manickvasagam, and A. K. Jain (1993), Extensional tectonics in the Himalayan orogen, Zaskar, NW India, in *Himalayan Tectonics*, edited by P. J. Treloar and M. P. Searle, *Spec. Publ. Geol. Soc.*, **74**, 445–459.
- Patriat, P., and J. Achache (1984), India-Eurasia collision chronology has implications for crustal shortening and driving mechanism of plates, *Nature*, **311**, 615–621, doi:10.1038/311615a0.
- Paul, S. K. (1998), Geology and tectonics of the Central Crystallines of northeastern Kumaon Himalaya, India, *J. Nepal Geol. Soc.*, **18**, 151–167.
- Rao, D. R., K. K. Sharma, and K. Gopalan (1995), Granitoid rock of Wangtu Gneissic Complex, Himachal Pradesh: An example of in situ fractional crystallisation and volatile action, *J. Geol. Soc. India*, **46**, 5–14.
- Ray, L., A. Bhattacharya, and S. Roy (2007), Thermal conductivity of Higher Himalayan Crystallines from Garhwal Himalaya, India, *Tectonophysics*, **434**, 71–79, doi:10.1016/j.tecto.2007.02.003.
- Rowley, D. B. (1996), Age of initiation of collision between India and Asia: A review of stratigraphic data, *Earth Planet. Sci. Lett.*, **145**, 1–13, doi:10.1016/S0012-821X(96)00201-4.
- Roy, A. B., and K. S. Vaidya (1988), Tectonometamorphic evolution of the Great Himalayan thrust sheets in Garhwal region, Kumaon Himalaya, *J. Geol. Soc. India*, **32**, 106–124.
- Schlup, M., A. Carter, M. Cosca, and A. Steck (2003), Exhumation history of eastern Ladakh revealed by $^{40}\text{Ar}/^{39}\text{Ar}$ and fission-track ages: The Indus-Tso Moriri transect, NW Himalaya, *J. Geol. Soc.*, **160**, 385–399, doi:10.1144/0016-764902-084.
- Searle, M. P., S. N. Roble, A. J. Hurford, and D. C. Rex (1999), Age of crustal melting, emplacement and exhumation history of the Shivaling leucogranite, Garhwal Himalaya, *Geol. Mag.*, **136**, 513–525, doi:10.1017/S00167656899002885.
- Searle, M. P., R. D. Law, L. Godin, K. P. Larson, M. J. Streule, J. M. Cottle, and M. J. Jessup (2008), Defining the Himalayan Main Central Thrust in Nepal, *J. Geol. Soc.*, **165**, 523–534, doi:10.1144/0016-76492007-081.
- Seitz, J. F., A. P. Tewari, and J. Obradovich (1976), A note on the absolute age of the tourmaline-granite, Arwa Valley, Garhwal Himalaya, *Geol. Soc. India Misc. Publ.*, **24**, 332–337.
- Singh, S., S. Claesson, A. K. Jain, H. Sjöberg, D. G. Gee, R. M. Manickvasagam, and P. G. Andreasson (1994), Geochemistry of the Proterozoic peraluminous granitoids from the Higher Himalayan Crystalline (HHC) and Jutogh Nappe, Himachal Pradesh, India, *J. Nepal Geol. Soc.*, **10**, 125.
- Sorkhabi, R. B., E. Stump, K. A. Foland, and A. K. Jain (1996), Fission-track and $^{40}\text{Ar}/^{39}\text{Ar}$ evidence for episodic denudation of the Gangotri granites in the Garhwal Higher Himalaya, India, *Tectonophysics*, **260**, 187–199, doi:10.1016/0040-1951(96)00083-2.
- Srivastava, P., and G. Mitra (1994), Thrust geometries and deep structure of the Outer and Lesser Himalaya, Kumaon and Garhwal (India): Implications for evolution of the Himalayan fold-and-thrust belt, *Tectonics*, **13**, 89–109, doi:10.1029/93TC01130.
- Stern, C. R., R. Kligfield, D. Schelling, N. S. Virdi, K. Futa, Z. E. Peterman, and H. Amini (1989), The Bhagirathi leucogranite of the high Himalaya (Garhwal, India): Age, petrogenesis, and tectonic implications, in *Tectonics of the Western Himalaya*, edited by L. L. Malinconico and R. J. Lillie, *Spec. Pap. Geol. Soc. Am.*, **232**, 33–45.
- Stüwe, K., L. White, and R. Brown (1994), The influence of eroding topography on steady-state isotherms: Application to fission track analysis, *Earth Planet. Sci. Lett.*, **124**, 63–74, doi:10.1016/0012-821X(94)00068-9.
- Thakur, V. C. (1980), Tectonics of the Central Crystallines of western Himalaya, *Tectonophysics*, **62**, 141–154, doi:10.1016/0040-1951(80)90142-0.
- Thiede, R. C., B. Bookhagen, J. R. Aarowsmith, E. R. Sobel, and M. R. Strecker (2004), Climatic control on areas of rapid exhumation along the southern

- Himalayan front, *Earth Planet. Sci. Lett.*, *222*, 791–806, doi:10.1016/j.epsl.2004.03.015.
- Thiede, R. C., J. R. Arrowsmith, B. Bookhagen, M. O. McWilliams, E. R. Sobel, and M. R. Strecker (2005), From tectonically to erosionally controlled development of the Himalayan orogen, *Geology*, *33*, 689–692, doi:10.1130/G21483.1.
- Thiede, R. C., T. A. Ehlers, B. Bookhagen, and M. R. Strecker (2009), Erosional variability along the NW Himalaya, *J. Geophys. Res.*, *114*, F01015, doi:10.1029/2008JF001010.
- Valdiya, K. S. (1980), *Geology of Kumaon Lesser Himalaya*, 291 pp., Wadia Inst. of Himalayan Geol., Dehradun, India.
- Vannay, J.-C., B. Grasemann, M. Rahn, W. Frank, A. Carter, V. Baudraz, and M. Cosca (2004), Miocene to Holocene exhumation of metamorphic crustal wedges in the NW Himalaya: Evidence for tectonic extrusion coupled to fluvial erosion, *Tectonics*, *23*, TC1014, doi:10.1029/2002TC001429.
- Whipp, D. M., and T. A. Ehlers (2007), Influence of groundwater flow on thermochronometer derived exhumation rates in the Nepalese Himalaya, *Geology*, *35*, 851–854, doi:10.1130/G23788A.1.
- Whipp, D. M. Jr., T. A. Ehlers, A. E. Blythe, K. W. Huntington, K. V. Hodges, and D. W. Burbank (2007), Plio-Quaternary exhumation history of the central Nepalese Himalaya: 2. Thermokinematic and thermochronometer age prediction model, *Tectonics*, *26*, TC3003, doi:10.1029/2006TC001991.
- Whipple, K., and B. J. Meade (2004), Controls on the strength of coupling among climate, erosion, and deformation in two-sided, frictional orogenic wedges at steady state, *J. Geophys. Res.*, *109*, F01011, doi:10.1029/2003JF000019.
- Whipple, K., and B. J. Meade (2006), Orogen response to changes in climatic and tectonic forcing, *Earth Planet. Sci. Lett.*, *243*, 218–228, doi:10.1016/j.epsl.2005.12.022.
- Yin, A. (2006), Cenozoic tectonic evolution of the Himalayan orogen as constrained by along-strike variation of structural geometry, exhumation history, and foreland sedimentation, *Earth Sci. Rev.*, *76*, 1–131, doi:10.1016/j.earscirev.2005.05.004.

A. Carter, School of Earth Sciences, Birkbeck College, University of London, Bloomsbury, Malet Street, London WC1E 7HX, UK.

R. C. Patel, Department of Geophysics, Kurukshetra University, Kurukshetra 136 119, India. (patelramesh_chandra@rediffmail.com)